An analytical approach to light scattering from small cubic and rectangular cuboidal nanoantennas

2013 New J. Phys. 15 063013

(http://iopscience.iop.org/1367-2630/15/6/063013)

New Journal of Physics
The open access journal for physics

An analytical approach to light scattering from small cubic and rectangular cuboidal nanoantennas

Enrico Massa[1], **Stefan A Maier and Vincenzo Giannini**
Blackett Laboratory, Department of Physics, Imperial College London, London SW7 2AZ, UK
E-mail: enrico.massa08@imperial.ac.uk

New Journal of Physics **15** (2013) 063013 (13pp)
Received 4 March 2013
Published 10 June 2013
Online at http://www.njp.org/
doi:10.1088/1367-2630/15/6/063013

Abstract. At optical frequencies metals behave as an electron plasma and conventional antenna designs need modifications when transferred to this regime. In contrast to antenna theory and to the effective wavelength picture, the position and width of the dipolar resonance of a rectangular cuboidal plasmonic nanoantenna scales nonlinearly with its length, width and height, as shown in this paper directly by analytical formulae. Moreover we show that the quality factor calculated for different sizes varies significantly with size, in contrast to the quasi-static approximation which predicts invariance. We present analytical expressions that provide a tool for direct and precise calculation of the dipolar plasmon resonance which can be applied to the antenna design process. These expressions enable both physical insight and the quick exploration of a wide range of parameters to tailor the plasmon resonance response or scattering by nanoparticles, for either metals or dielectrics, for numerous promising applications in optical sensor, photovoltaic and light emitting device design.

S Online supplementary data available from stacks.iop.org/NJP/15/063013/mmedia

[1] Author to whom any correspondence should be addressed.

Contents

1. Introduction

Antenna technology, which was developed for radio and micro-wave frequencies, manipulates the electromagnetic field on a subwavelength scale, providing a means to interface propagating and localized fields [1]. The control of light, however, has typically been accomplished using devices much larger than the wavelength, such as lenses, mirrors, gratings, etc, and, therefore, has been intrinsically limited by diffraction. Recently, advances in nano-optics and plasmonics have enabled the creation of nanoscale antennas that work at optical frequencies, with the aim to create analogous devices to those that work at larger wavelengths.

Nanoantennas have been shown to have many possible applications, such as in enhancing light–emitter interactions [2], high-resolution microscopy and spectroscopy [3], optical sensors [4–9], THz plasmonics [10], photovoltaics and solar cells [11–14], solid state lighting [15] and lasing [16]. Currently, much research is focused on scaling the established concepts of antenna theory to the optical regime to facilitate optical antenna design.

One of the main difficulties is that at optical frequencies the incident radiation penetrates into the metal and is not perfectly reflected. This gives rise to coherent oscillations of the free-electron gas, i.e. to a plasmon resonance [17]. The response of a metal at optical frequencies is, therefore, very different from that of a perfect conductor, as is assumed in antenna theory. In order to obtain meaningful results at optical frequencies, it is then necessary to take into account the dielectric function of the metal. For metallic spheres, Mie theory provides the solution of the scattering problem, and ellipsoids can be solved analytically in the quasi-static approximation [18, 19]. Fuchs and Ruppin demonstrated a method to calculate the electromagnetic cross sections of cubes in the electrostatic limit [20, 21] although this method does not consider radiative damping or any other retardation effects. In general, no solutions are available for other geometries. A simple analytical description of the scattering from rectangular cuboidal antennas (or any other shaped scatterer [22]) could allow a deeper understanding and it would provide a simple method for studying the scattering phenomena without resorting to complex and time consuming simulations.

Cubic [14, 23–25], or generally rectangular cuboidal [7, 8, 26–28], single nanoparticles, dimers [29–31] or arrays of nanoparticles of different shapes have been widely studied due to their tunability and ease of fabrication. For rod nanoantennas, an effective wavelength picture has been derived, in which the optical antenna no longer responds to the external wavelength, but to a shorter effective wavelength λ_{eff} which depends on the material properties via a linear relationship $\lambda_{\mathrm{eff}} = n_1 + n_2[\lambda/\lambda_{\mathrm{p}}]$, where λ_{p} is the plasma wavelength and n_1 and n_2 are coefficients that depend on the properties of the antenna and the surrounding dielectric [32].

This picture is more effective in the infra-red regime [33] but it fails to provide an accurate solution in the interesting range of optical frequencies, where structures are usually in the range of 100 nm or less. Moreover, under the quasi-static approximation, theory predicts that the Q factor is determined solely by the complex dielectric function of the metal and is independent of the nanostructure form or dielectric environment [34]. We will show that this is not the case for rectangular cuboidal nanoantennas usually used, due mainly to radiation losses, which are neglected in the quasi-static approximation.

In this paper, we provide general analytical formulae for the calculation of the scattering properties of a rectangular cuboid (which, from now on, will be simply referred as cuboid) inside a medium, in the assumption that the field inside the cuboid is constant, corrected for the charges at the vertices. From these formulae, we consider the scaling of the position and width and of the value of the peak of the extinction efficiency of the resonance with the length, width and height of the cuboid. The results improve upon those given by the effective wavelength model for metal structures smaller than 100 nm and illustrate the scaling and behaviour of the Q factor of the resonance, highlighting its change with the nanostructure geometry. The results have been compared for a wide range of geometrical parameters against finite element method (FEM) simulations using COMSOL, obtaining a very good agreement.

1.1. Formalism

Consider a rectangular cuboid of volume V placed with its centre at the origin, as shown in figure 1, with length $L_a = 2a$, width $L_b = 2b$ and height $L_c = 2c$. The cuboid is composed of a material with a complex, wavelength dependent, dielectric function ϵ and is surrounded by a background material with a dielectric constant ϵ_B. The incident electromagnetic field is a plane wave $\mathbf{E}(\mathbf{r}) = \mathbf{E}_0\, \mathrm{e}^{\mathrm{i}k_\mathrm{B}z}$, where, in all the following, it will be assumed the time varying dependence of the field is given by $\mathrm{e}^{-\mathrm{i}\omega t}$. The electric field $\mathbf{E}_0$ is along the x direction and the wave-vector in the background is $k_\mathrm{B} = \sqrt{\epsilon_\mathrm{B}}k_0 = \sqrt{\epsilon_\mathrm{B}}\omega/c$. A first analytical expression is obtained using the Meier–Wokaun approach [35]. Later we improve the result by means of the Green function formalism. This formalism [36, 37] has been used in order to obtain an expression for the scattered field in the far field under the assumption that the electric field inside the cuboid is constant and is given by the field at the central point previously obtained with the Meier–Wokaun approach. The field at the central point is calculated by considering the effects of depolarization in the volume and of the charges induced at the vertices. We can consider this as the zero order of a modal expansion and this can be considered as an educated guess confirmed *a posteriori*. It is important to point out that we model only the dipolar order and, secondly, that using the experimental dielectric functions of metals instead of the Drude formula (particularly gold), the resonances higher than the dipolar are strongly suppressed by the losses, making this assumption a good approximation. Moreover this approximation is reasonable considering the small scale of the nanoparticles and the fact that gives the exact solution for a small sphere [35]. A full derivation of the resulting equations is provided in the supporting information.

1.1.1. Electric field inside the nanoantenna. Starting from the Meier–Wokaun [35] approach for a sphere, the electric field inside a cuboidal nanoparticle can be approximated by considering the necessary corrections due to the induced charges (see the appendix). The electric field inside

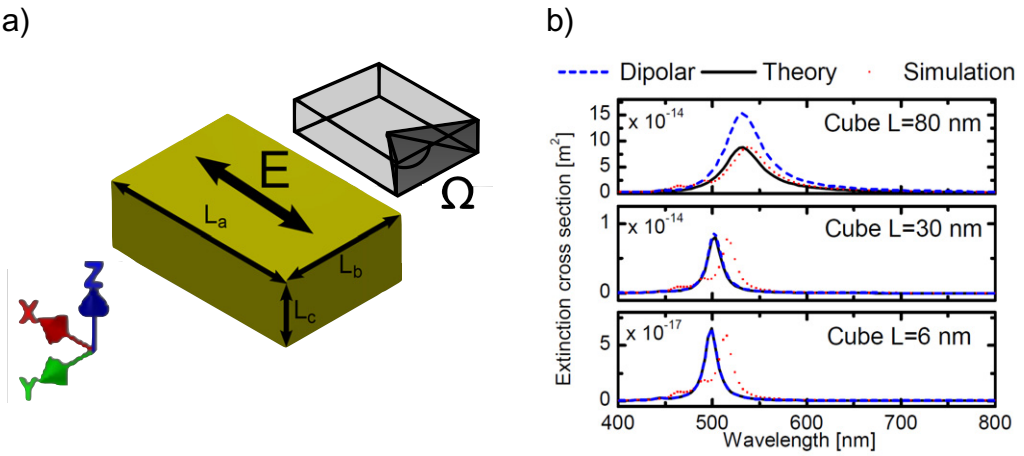

Figure 1. (a) Sketch of a cuboid with sides $L_a = 2a$ along the x direction, $L_b = 2b$ along the y direction and $L_c = 2c$ along the z direction. The electric field of the incident plane wave is polarized along the x direction. The centre of the cuboid is placed at zero of the coordinate system. The solid angle Ω of equation (2) is also shown in dark. (b) Comparison between the extinction cross sections for cubes of side lengths $L = 6$, 30 and 80 nm calculated using our theory (solid black line) and the ones obtained by FEM simulations (dotted red line). Results obtained using the dipolar approximation (dashed blue line), which works best for small nanoantennas, are also shown. The smaller peaks appearing between 450 and 500 nm in the numerical simulation curves are higher order modes.

the nanoantenna may then be expressed as

$$E_{x,\mathrm{int}} = \frac{E_0}{1 - \frac{\epsilon - \epsilon_\mathrm{B}}{4\pi\epsilon_\mathrm{B}}\left[-2\Omega - \delta + \frac{k_\mathrm{B}^2}{2}\beta + \frac{16}{3}\mathrm{i}k_\mathrm{B}^3 abc\right]}, \tag{1}$$

where E_0 is the incident field, Ω is the solid angle subtended by the side perpendicular to the polarization axis of the cuboid (the x-axis in this case), i.e. the side L_b–L_c (see figure 1(a)), which gives the singular contribution of the dyadic [37], and is expressed by

$$\Omega = 4\arcsin\left(\frac{bc}{\sqrt{(a^2+b^2)(a^2+c^2)}}\right), \tag{2}$$

β is the dynamic geometrical depolarization factor, defined by equation (A.3) in the appendix section and with full derivation in the supplementary data (available from stacks.iop.org/NJP/15/063013/mmedia). For a cube, it is expressed by $\beta_\mathrm{cube} \approx 12.6937a^2$. δ is a term that takes into account the polarization charges at the planar ends of the cuboid orthogonal to the x direction, and is expressed by

$$\delta = \frac{8abc}{(a^2+b^2+c^2)^{3/2}}\frac{\epsilon_\mathrm{B}}{\epsilon}. \tag{3}$$

Lastly, the term $\frac{16}{3}\mathrm{i}k_\mathrm{B}^3 abc$ constitutes the radiative correction to the field. Note that equation (1) takes into account the effect of depolarization from all dipole moments surrounding the centre [35].

1.1.2. Dipolar approximation. The above expression for the internal electric field can be used together with the dipolar expressions for the scattering and absorption cross sections:

$$\sigma_{\text{sca}} = \frac{k_{\text{B}}^4}{6\pi}|\alpha|^2 \tag{4}$$

and

$$\sigma_{\text{abs}} = k_{\text{B}}\Im(\alpha), \tag{5}$$

respectively, along with the polarizability α, obtained from the dipole moment $\mathbf{p} = \epsilon_0\epsilon_{\text{B}}\alpha\mathbf{E}_0$, and defined as

$$\alpha = 8abc\frac{(\epsilon-\epsilon_{\text{B}})E_{x,\text{int}}}{\epsilon_{\text{B}}E_0} = \frac{8abc}{\frac{\epsilon_{\text{B}}}{\epsilon-\epsilon_{\text{B}}} - \frac{1}{4\pi}\left[-2\Omega - \delta + \frac{k_{\text{B}}^2}{2}\beta + \frac{16}{3}\text{i}k_{\text{B}}^3 abc\right]}, \tag{6}$$

to obtain very simple expressions for the cross sections, with the extinction cross section defined as $\sigma_{\text{ext}} = \sigma_{\text{sca}} + \sigma_{\text{abs}}$.

1.1.3. Far-field scattering. Although the field inside the nanoantenna allows us to derive simple dipolar formulae for the scattering, absorption and extinction cross sections, a more accurate result is obtained by now considering scattering in the far field using the Green function formalism (see the appendix), since in this case we do not assume that the scatterer is a point dipole. Starting with equation (A.6) and considering the field inside the nanoantenna given by equation (1), the scattering cross section is obtained as

$$\sigma_{\text{sca}} = \frac{1}{E_0^2}\int_S \text{d}S\, r^2\left|\mathbf{E}_{\text{sca}}^{\text{FF}}\right|^2 = \frac{k_0^4|\Delta\epsilon|^2}{15\pi E_0^2}\left\{\frac{8}{63}a^2b^2c^2[1260 - k_{\text{B}}^2(84a^2+168b^2+168c^2) + k_{\text{B}}^4(3a^4+9b^4+9c^4+4a^2b^2+4a^2c^2+6b^2c^2)]|E_{x,\text{int}}|^2\right\}, \tag{7}$$

where $\Delta\epsilon = \epsilon - \epsilon_{\text{B}}$. A derivation is shown in the appendix section. The extinction cross section is also obtained from the scattered field by means of the optical theorem using equation (A.9)

$$\sigma_{\text{ext}} = \frac{4\pi}{k_{\text{B}}^2 E_0}\Re\left[\frac{-\text{i}k_{\text{B}}r}{\text{e}^{\text{i}k_{\text{B}}r}}E_{x,\text{sca}}\right]_{\substack{x,y=0\\ z\to+\infty}} = -\frac{k_0^2}{k_{\text{B}}E_0}\Re[\text{i}\Delta\epsilon E_{x,\text{int}}]\left(8abc - \frac{4k_{\text{B}}^2}{3}abc^3\right), \tag{8}$$

where $\Re$ is the real part. The absorption cross section is calculated by using the expression $\sigma_{\text{abs}} = \sigma_{\text{ext}} - \sigma_{\text{sca}}$.

In order to compare with simulation results, we consider the case of gold (Au) nanoantennas. The dielectric function of the Au has been expressed using Drude model, which fits well to the experimental dielectric function but neglects the interband transition region. Note that this is chosen only for convenience during the comparison. In fact, the model works with an arbitrary dielectric function, ϵ, and therefore also with any experimental dielectric function. In particular, we have simulated gold using the following expression:

$$\epsilon(\omega) = \epsilon_\infty - \frac{\omega_{\text{P}}^2}{\omega(\omega+\text{i}\gamma)}, \tag{9}$$

where $\epsilon_\infty = 10.7026$, ω_{P} is the plasma frequency ($\omega_{\text{P}} = 1.3748\times10^{16}$ Hz) and γ is the collision frequency ($\gamma = 1.1738\times10^{14}$ Hz). We will show that the analytic formulae agree very well with numerical calculations over a wide range of values, from just a few to ≈100 nm.

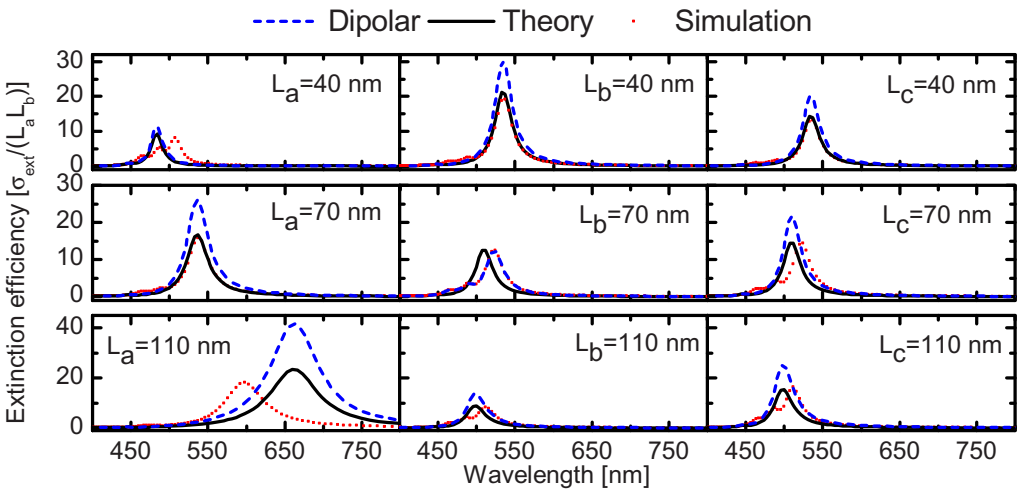

Figure 2. Comparison between the extinction efficiencies $\sigma_{\text{ext}}/(L_a L_b)$ for cuboids of length, width and height equal to 40, 70 and 110 nm (as indicated) calculated from our theory (equation (8), solid black line), the dipolar approximation (equations (4) and (5), dashed blue line) and the ones obtained by FEM simulations (dotted red line). The dimensions of either L_a, L_b, L_c which are not indicated in the inset on each figure are equal to 60 nm. The smaller peaks appearing between 450 and 500 nm in the numerical simulation curves are higher order modes.

2. Results and discussion

The geometry of the scattering problem is shown in figure 1(a), where the electric field is incident in the x direction. Figure 1(b) shows the comparison between the extinction cross section for cubes of different side lengths L calculated using our approach (equation (8), solid black line), our dipolar approximation (equations (4) and (5), dashed blue line) and that obtained by numerical FEM simulations using COMSOL (dotted red line). The plasmon resonance appears as a single main peak that red-shifts and widens with increasing the size of the particle. Smaller peaks appear between 450 and 500 nm in the simulations curves due to higher order modes.

Figure 2 shows the comparison for cuboids of different side lengths between our theory (equation (8), solid black line), our dipolar approximation (equations (4) and (5), dashed blue line) and the same obtained by FEM simulations (dotted red line). To avoid numerical errors due to the discontinuity at the surface in the FEM simulations, all sharp corners and edges of the cuboid have been slightly smoothed by spherical or cylindrical surfaces of radius $R = L/10$ where L is the shortest side length. The total scattering cross sections were obtained by integrating the scattered power flux over an enclosing spherical surface outside the cuboid, while the absorption cross sections were determined by integrating the Ohmic heating within the cuboid. Each numerical simulation curve shows a strong dipolar resonance, as well as several weak higher order resonant modes.

As shown in figures 1 and 2, theory and FEM simulations are generally in good agreement. Both expressions (8), (4) and (5) give good information about the plasmonic resonance. In particular, equation (8) predicts well the position of the main dipolar plasmon resonance peak

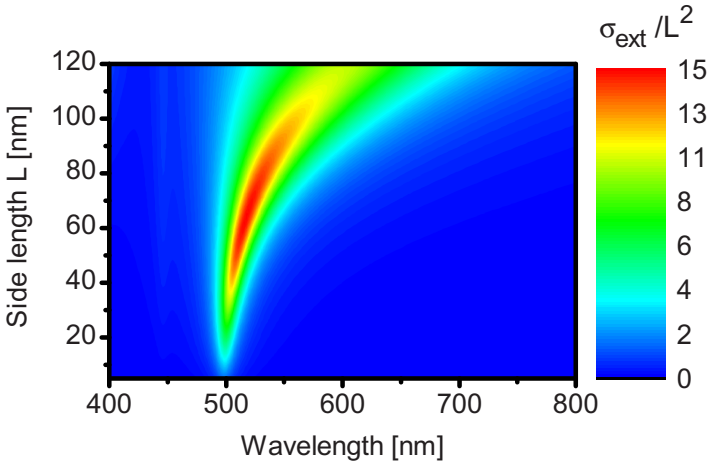

Figure 3. Colour plot of the extinction efficiency σ_{ext}/L^2 of cubes of different side length L against the wavelength. The peak of the plasmon resonance shows a nonlinear shift with length up to 80 nm. Results are calculated using equation (8).

and very well its width and strength for particles of only few nm to more than 100 nm. We can also see that our model works better for larger particles, while, for smaller ones, we notice a small blue-shift of the resonance of approximately 20 nm. This is due to the fact that the constant field approximation does not exactly capture the excited modes inside the cuboid.

The good agreement of these analytical results with complex simulations means that the analytic expression provides a simple, quick, yet accurate method of evaluating the effect of varying size parameters on the plasmon resonance. For example, one can study the behaviour of the resonance when varying the cube side length. Interestingly, one discovers that the plasmon resonance peak shifts nonlinearly with the length, as shown very clearly by figure 3, which shows the extinction efficiency, σ_{ext}/L^2, for cubes of different side length L as a function of the wavelength. As expected, the resonance red-shifts and broadens when increasing the length of the structure, due to the increases in the effective wavelength and radiative losses, respectively. From figure 3 one can see the existence of two scaling regimes, one nonlinear for side lengths smaller than approximately 80 nm and one linear for side lengths larger than that.

It is also possible to check quickly the tuning of the plasmon resonance to a desired position by changing any of the three dimensions of the cuboid. In particular, as shown in figure 4, the plasmon resonance position scales nonlinearly when changing the length, width and height of the cuboid, in contrast to the predictions of the effective wavelength model which show a linear scaling with the length. In particular, the squeezing of the width and height causes a significant red-shift of the resonance.

These results are important to establish design rules for transferring antenna technology to the optical regime. This technique can then be extended to complex designs composed, for instance, of many antenna rods such as Yagi–Uda antennas.

Another interesting parameter to characterize a plasmon resonance is the quality (Q) factor, which is inversely proportional to the width of the resonance. Figure 5(a) shows a colour plot of the Q factor with changing length, L_a, and width, L_b, with a fixed height $L_c = 50$ nm. The region with $L_a < 40$ nm shows the highest Q factor, above 35, while the lowest Q factor of about 10 is in the region with $L_a > 60$ nm and $L_b > 40$ nm. For sensing applications, it is often

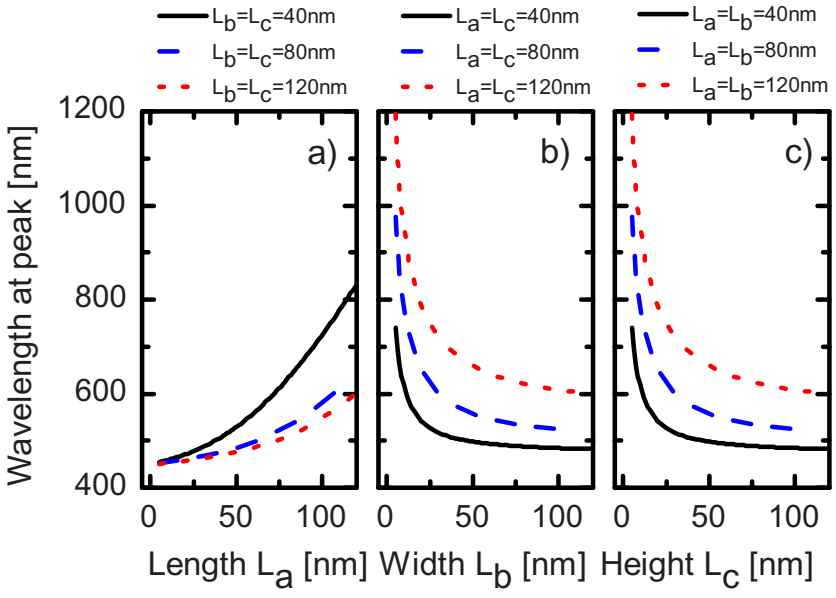

Figure 4. Wavelength position of the maximum of the plasmon resonance for cuboids. Changing the length, width and height results in a significant nonlinear behaviour. Results are calculated using equation (8).

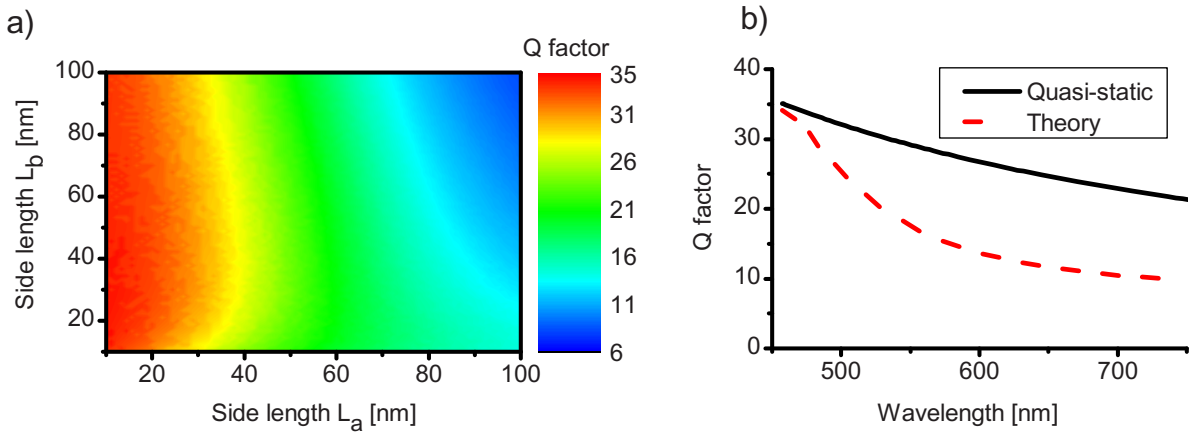

Figure 5. (a) Colour plot of the Q factor of the plasmon resonance for cuboids, changing the length L_a and width L_b with height $L_c = 50\,\text{nm}$. (b) Q factor of the plasmon resonance for cuboids, changing the length L_a between 10 and 120 nm, with $L_b = L_c = 50\,\text{nm}$. Quasi-static theory is always above the values from our theory, because it neglects radiation losses. Results are calculated using equation (8).

important to tune the plasmon resonance to a specified region and to have a resonance with the highest Q factor achievable in order to have the greatest sensitivity. Quasi-static theory predicts that with losses occurring only in the metal part of the nanostructure, the Q factor may be

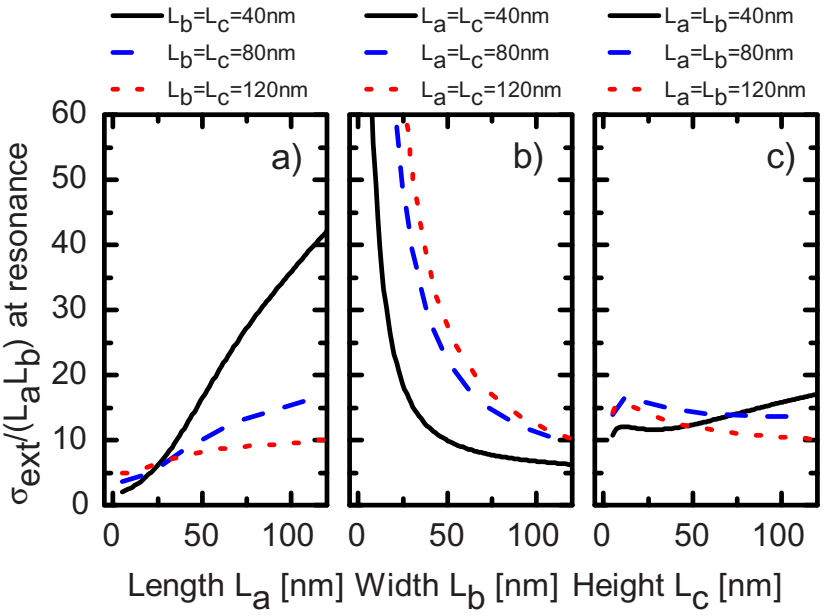

Figure 6. Maximum of the extinction efficiency $\sigma_{\text{ext}}/(L_a L_b)$ at the plasmon resonance for cuboids with changing length L_a, width L_b and height L_c. Results are calculated using equation (8).

expressed as

$$Q = \frac{\omega}{2\epsilon''}\frac{\mathrm{d}\epsilon'}{\mathrm{d}\omega} = \frac{\omega^3}{\gamma(\omega^2+\gamma^2)}, \tag{10}$$

where ϵ' and ϵ'' are the real and imaginary parts of ϵ, respectively, and we have used the definition of ϵ from the Drude model (equation (9)). Note that equation (10) neglects losses due to radiation, which effectively increase the loss coefficient ϵ'', making the Q factor smaller. Figure 5(b) shows the comparison between the results predicted by equation (10) and the values calculated using our formalism from $Q = \omega/\Delta\omega$, where $\Delta\omega$ is the FWHM of the plasmon resonance, for cuboids of different side lengths. The quasi-static theory always produces values above those from our theory because it neglects radiation losses, and, in the worst case, can be off by up to a factor of 2 compared to the value from our theory.

Another important parameter for sensing is the figure of merit (FOM) [9], which is defined as $\text{FOM} = \frac{\partial\lambda}{\partial n}/\Delta\lambda$, where $\Delta\lambda$ is the resonance width and $\frac{\partial\lambda}{\partial n}$ is the shift of the resonance wavelength upon a change of the refractive index of the surrounding medium n. Clearly, for a known background refractive index, upon a shift ∂n of its value which causes a shift of the peak of the plasmon resonance $\partial\lambda$, equation (8) makes it possible to obtain $\frac{\partial\lambda}{\partial n}$ and the width of the resonance $\Delta\lambda$. In this way we have a direct and useful method to obtain the FOM.

Finally, we consider how the maximum of the extinction efficiency, $\sigma_{\text{ext}}/(L_a L_b)$, shown in figure 6 varies with changing length, width and height. This provides important information on how to increase the extinction efficiency at resonance for the same volume of material. Changing the length L_a, the extinction efficiency monotonically increases, in some cases to very large values (over 40), whereas changing the width L_b has the inverse effect, since we obtain large

values only for small widths. Changing the height L_c has a small mixed effect with an increase or decrease for smaller height L_c depending of the values of the length and width. This can be used for the fabrication of strongly scattering nanoantennas, with low absorption, since it shows the marginal contribution of a change in size of each dimension.

3. Conclusions

In summary, we have derived analytical expressions for the extinction, scattering, and absorption cross sections of a rectangular cuboid, showing a nonlinear scaling of the plasmon resonance position, width and extinction efficiency. This enables one to precisely downscale antenna designs to optical frequencies by enabling a convenient calculation of the dipolar plasmon resonance. Moreover, the formalism can be applied to the design of strongly scattering nanoantennas with low absorption and to the analysis of operational parameters such as the Q factor and FOM. In fact, we have shown that the Q factor changes significantly with the dimensions of the cuboid, in contrast to the quasi-static approximation, which predicts invariance with size. This enables the simultaneous tailoring of the Q factor of the plasmon resonance and of the FOM for sensing applications.

Acknowledgments

This work was supported by EPSRC and the Leverhulme Trust. EM thanks Tyler Roschuk for helpful discussions.

Appendix

A.1. Near-field

We assume that the polarization of the cuboid is homogeneous in its volume. Obviously, this is not strictly correct for a cuboid, but the result will be corrected to take into account the induced charges at the vertexes. More in details, the polarization is given by

$$\mathbf{P} = \epsilon_0(\epsilon - \epsilon_\mathrm{B})(\mathbf{E}_0 + \mathbf{E}_\mathrm{dep}), \tag{A.1}$$

where $\mathbf{E}_\mathrm{dep}$ is the depolarization field generated by the matter surrounding a point in the volume. Following Meier and Wokaun [35], the electric field produced by a retarded dipole $\mathrm{d}\mathbf{p}(\mathbf{r})$ oriented along x at the centre of the cuboid parallel to the x axis, is expressed by

$$\mathrm{d}E_{\mathrm{dep},x} = \frac{1}{4\pi\epsilon_0\epsilon_\mathrm{B}}\left[\frac{1}{r^3}(3\cos^2\theta - 1) + \frac{k_\mathrm{B}^2}{2r}(\cos^2\theta + 1) + \frac{2}{3}\mathrm{i}k_\mathrm{B}^3\right] P_x\,\mathrm{d}V. \tag{A.2}$$

By changing coordinates and integrating this expression over the cube we are left with three terms. The first term is equation (2), the second is β expressed by

$$\beta = \int_{-c}^{c}\int_{-b}^{b}\int_{-a}^{a} \frac{1}{\sqrt{x^2+y^2+z^2}}\left(1 + \frac{x^2}{x^2+y^2+z^2}\right)\mathrm{d}x\,\mathrm{d}y\,\mathrm{d}z, \tag{A.3}$$

which can be expressed analytically with a rather long expression, given in the supporting information. The third term can be integrated in a simple way to give $\frac{16}{3}\mathrm{i}k_{\mathrm{B}}^3 abc$, which takes into account the radiative correction to the field. In this way we obtained

$$E_{\mathrm{dep},x} = \frac{1}{4\pi\epsilon_0\epsilon_{\mathrm{B}}}\left[-2\Omega + \frac{k_{\mathrm{B}}^2}{2}\beta + \frac{16}{3}\mathrm{i}k_{\mathrm{B}}^3 abc\right]P_x. \tag{A.4}$$

By considering also the effect of polarization charges at the planar ends of the cuboid and orthogonal to the x direction, another term in the expression of $E_{\mathrm{dep},x}$ appears. Using equation $\mathbf{P}\cdot\mathbf{n} = \sigma$ where σ is the surface charge at the planar ends and $\mathbf{n}$ is the external normal vector, we obtain that the charge at the surfaces, which we consider concentrated at each vertex, is given by $q = P_x bc$ for each vertex, where q is positive in the $x = a$ and negative in the $x = -a$ planar surfaces. The contribution to the field along x at the centre of the cuboid given by the charges at the vertices is

$$E_{\mathrm{vert},x} = -\frac{8}{4\pi\epsilon_0\epsilon}\frac{abcP_x}{(a^2+b^2+c^2)^{3/2}}, \tag{A.5}$$

where we have taken into account the projection of the electric field along x generated by the charges. Using the expression of equations (A.4) and (A.1) and by defining δ as equation (3), we are left with the expression of equation (1), which gives a corrected expression that takes into account the induced charges at the surface of the cuboid.

A.2. Far-field

Consider the expression of the scattered field given by the Green formulation, where $\overleftrightarrow{\mathbf{G}}_{\mathrm{FF}}$ is the Green function in the far field:

$$\mathbf{E}_{\mathrm{sca}}^{\mathrm{FF}}(\mathbf{r}) = \int_V \mathrm{d}\mathbf{r}'\,\overleftrightarrow{\mathbf{G}}_{\mathrm{FF}}\; k_0^2\,\Delta\epsilon\,\mathbf{E}(\mathbf{r}') = \int_V \mathrm{d}\mathbf{r}'\frac{\mathrm{e}^{\mathrm{i}k_{\mathrm{B}}R}}{4\pi R}\left[\overleftrightarrow{\mathbf{I}} - \frac{\mathbf{RR}}{R^2}\right]k_0^2\,\Delta\epsilon\,\mathbf{E}(\mathbf{r}'), \tag{A.6}$$

where $\mathbf{R} = \mathbf{r} - \mathbf{r}'$, $R = |\mathbf{r} - \mathbf{r}'|$ and $\Delta\epsilon = \epsilon - \epsilon_{\mathrm{B}}$, were ϵ is the dielectric function of our antenna and ϵ_{B} that of the surrounding medium.

Given that the structure is symmetric in the $x-z$ and $y-z$ planes, it can be shown that the electric field fulfils the following symmetry relationships:

$$\begin{cases} E_x(x) = E_x(-x), \\ E_x(y) = E_x(-y), \end{cases} \quad \begin{cases} E_y(x) = -E_y(-x), \\ E_y(y) = -E_y(-y), \end{cases} \quad \begin{cases} E_z(x) = -E_z(-x), \\ E_z(y) = E_z(-y), \end{cases} \tag{A.7}$$

which are valid for each $z =$ constant plane. Our main assumption is that the field inside the cuboid is given by equation (1). With this assumption and by doing the approximations of $1/R \approx 1/r$, $R \approx r - r'\cos\gamma$, where γ is the angle between $\mathbf{r}$ and $\mathbf{r}'$, and $\left[1 - \frac{\mathbf{RR}}{R^2}\right] \approx \left[1 - \frac{\mathbf{rr}}{r^2}\right]$ since the higher order terms generate contributions that go to zero faster than $1/r^2$ which are negligible in the far field, one obtains

$$E_{\mathrm{sca}}^{\mathrm{FF}} = \frac{\mathrm{e}^{\mathrm{i}k_{\mathrm{B}}r}k_0^2\,\Delta\epsilon}{4\pi r}\left[\overleftrightarrow{\mathbf{I}} - \frac{\mathbf{rr}}{r^2}\right]\mathbf{E}_{\mathrm{int}}\int_V \mathrm{d}\mathbf{r}'\,\mathrm{e}^{-\mathrm{i}k_{\mathrm{B}}r'\cos\gamma}. \tag{A.8}$$

If we consider an internal electric field only along the x direction (see figure 1) $\mathbf{E}_{\mathrm{int}} = (E_{x,\mathrm{int}}, 0, 0)$, it is possible to derive the following expressions of the scattered electric field in

the far field by direct integration of each term of the exponential series:

$$E^{\mathrm{FF}}_{x,\mathrm{sca}} = \frac{\mathrm{e}^{\mathrm{i}k_{\mathrm{B}}r}k_0^2\,\Delta\epsilon}{4\pi r}\left\{\left[1-\frac{x^2}{r^2}\right]E_{x,\mathrm{int}}\left(8abc-\frac{4k_{\mathrm{B}}^2}{3r^2}\left[a^3bcx^2+ab^3cy^2+abc^3z^2\right]\right)+O(k_{\mathrm{B}}^3)\right\},$$

$$E^{\mathrm{FF}}_{y,\mathrm{sca}} = \frac{\mathrm{e}^{\mathrm{i}k_{\mathrm{B}}r}k_0^2\,\Delta\epsilon}{4\pi r}\left\{-\frac{yx}{r^2}E_{x,\mathrm{int}}\left(8abc-\frac{4k_{\mathrm{B}}^2}{3r^2}\left[a^3bcx^2+ab^3cy^2+abc^3z^2\right]\right)+O(k_{\mathrm{B}}^3)\right\}, \quad \text{(A.9)}$$

$$E^{\mathrm{FF}}_{z,\mathrm{sca}} = \frac{\mathrm{e}^{\mathrm{i}k_{\mathrm{B}}r}k_0^2\,\Delta\epsilon}{4\pi r}\left\{-\frac{zx}{r^2}E_{x,\mathrm{int}}\left(8abc-\frac{4k_{\mathrm{B}}^2}{3r^2}\left[a^3bcx^2+ab^3cy^2+abc^3z^2\right]\right)+O(k_{\mathrm{B}}^3)\right\}.$$

From the scattered field, equations (7) and (8) give the scattering and extinction cross sections.

References

[1] Bharadwaj P, Deutsch B and Novotny L 2009 *Adv. Opt. Photon.* **1** 438–83
[2] Giannini V, Fernández-Domínguez A I, Sonnefraud Y, Roschuk T, Fernández-García R and Maier S A 2010 *Small* **6** 2498–507
[3] Farahani J N, Pohl D W, Eisler H J and Hecht B 2005 *Phys. Rev. Lett.* **95** 017402
[4] Schuck P J, Fromm D P, Sundaramurthy A, Kino G S and Moerner W E 2005 *Phys. Rev. Lett.* **94** 017402
[5] Mühlschlegel P, Eisler H-J, Martin O J F, Hecht B and Pohl D W 2005 *Science* **308** 1607–9
[6] Zhang S, Bao K, Halas N J, Xu H and Nordlander P 2011 *Nano Lett.* **11** 1657–63
[7] Aouani H, Šípová H, Rahmani M, Navarro-Cia M, Hegnerová K, Homola J, Hong M and Maier S A 2013 *ACS Nano* **7** 669–75
[8] Lee S Y, Hung L, Lang G S, Cornett J E, Mayergoyz I D and Rabin O 2010 *ACS Nano* **4** 5763–72
[9] Offermans P, Schaafsma M C, Rodriguez S R K, Zhang Y, Crego-Calama M, Brongersma S H and Gómez-Rivas J 2011 *ACS Nano* **5** 5151–7
[10] Giannini V, Berrier A, Maier S A, Sánchez-Gil J A and Rivas J G 2010 *Opt. Express* **18** 2797–807
[11] Li X, Hylton N P, Giannini V, Lee K H, Ekins-Daukes N J and Maier S A 2011 *Opt. Express* **19** A888–A896
[12] Mokkapati S and Catchpole K R 2012 *J. Appl. Phys.* **112** 101101
[13] Derkacs D, Lim S H, Matheu P, Mar W and Yu E T 2006 *Appl. Phys. Lett.* **89** 093103
[14] Macpherson H A and Stoldt C R 2012 *ACS Nano* **6** 8940–9
[15] Mertens H, Biteen J S, Atwater H A and Polman A 2006 *Nano Lett.* **6** 2622–5
[16] Cubukcu E, Kort E A, Crozier K B and Capasso F 2006 *Appl. Phys. Lett.* **89** 093120
[17] Maier S A 2007 *Plasmonics: Fundamentals and Applications* (Berlin: Springer)
[18] Bohren C F and Huffman D R 1983 *Absorption and Scattering of Light by Small Particles* (New York: Wiley)
[19] Moroz A 2009 *J. Opt. Soc. Am.* B **26** 517–27
[20] Fuchs R 1975 *Phys. Rev.* B **11** 1732–40
[21] Ruppin R 1996 *Z. Phys.* D **36** 69–71
[22] Pendry J B, Aubry A, Smith D R and Maier S A 2012 *Science* **337** 549–52
[23] Chan H, Demortière A, Vukovic L, Král P and Petit C 2012 *ACS Nano* **6** 4203–13
[24] Haggui M, Dridi M, Plain J, Marguet S, Perez H, Schatz G C, Wiederrecht G P, Gray S K and Bachelot R 2012 *ACS Nano* **6** 1299–307
[25] Chen H Y, He C L, Wang C Y, Lin M H, Mitsui D, Eguchi M, Teranishi T and Gwo S 2011 *ACS Nano* **5** 8223–9
[26] Grillet N, Manchon D, Bertorelle F, Bonnet C, Broyer M, Cottancin E, Lermé J, Hillenkamp M and Pellarin M 2011 *ACS Nano* **5** 9450–62
[27] Cortie M B, Liu F, Arnold M D and Niidome Y 2012 *Langmuir* **28** 9103–12
[28] Sherry L J, Chang S H, Schatz G C, Van Duyne R P, Wiley B J and Xia Y 2005 *Nano Lett.* **5** 2034–8
[29] Jain P K and El-Sayed M A 2007 *Nano Lett.* **7** 2854–8

[30] Rolly B, Stout B and Bonod N 2011 *Phys. Rev.* B **84** 125420
[31] Hohenester U and Krenn J 2005 *Phys. Rev.* B **72** 195429
[32] Novotny L 2007 *Phys. Rev. Lett.* **98** 266802
[33] Bryant G W, García de Abajo F J and Aizpurua J 2008 *Nano Lett.* **8** 631–6
[34] Wang F and Shen Y R 2006 *Phys. Rev. Lett.* **97** 206806
[35] Meier M and Wokaun A 1983 *Opt. Lett.* **8** 581–3
[36] Martin O J F and Piller N B 1998 *Phys. Rev.* E **58** 3909–15
[37] Yaghjian A D 1980 *Proc. IEEE* **68** 248–63